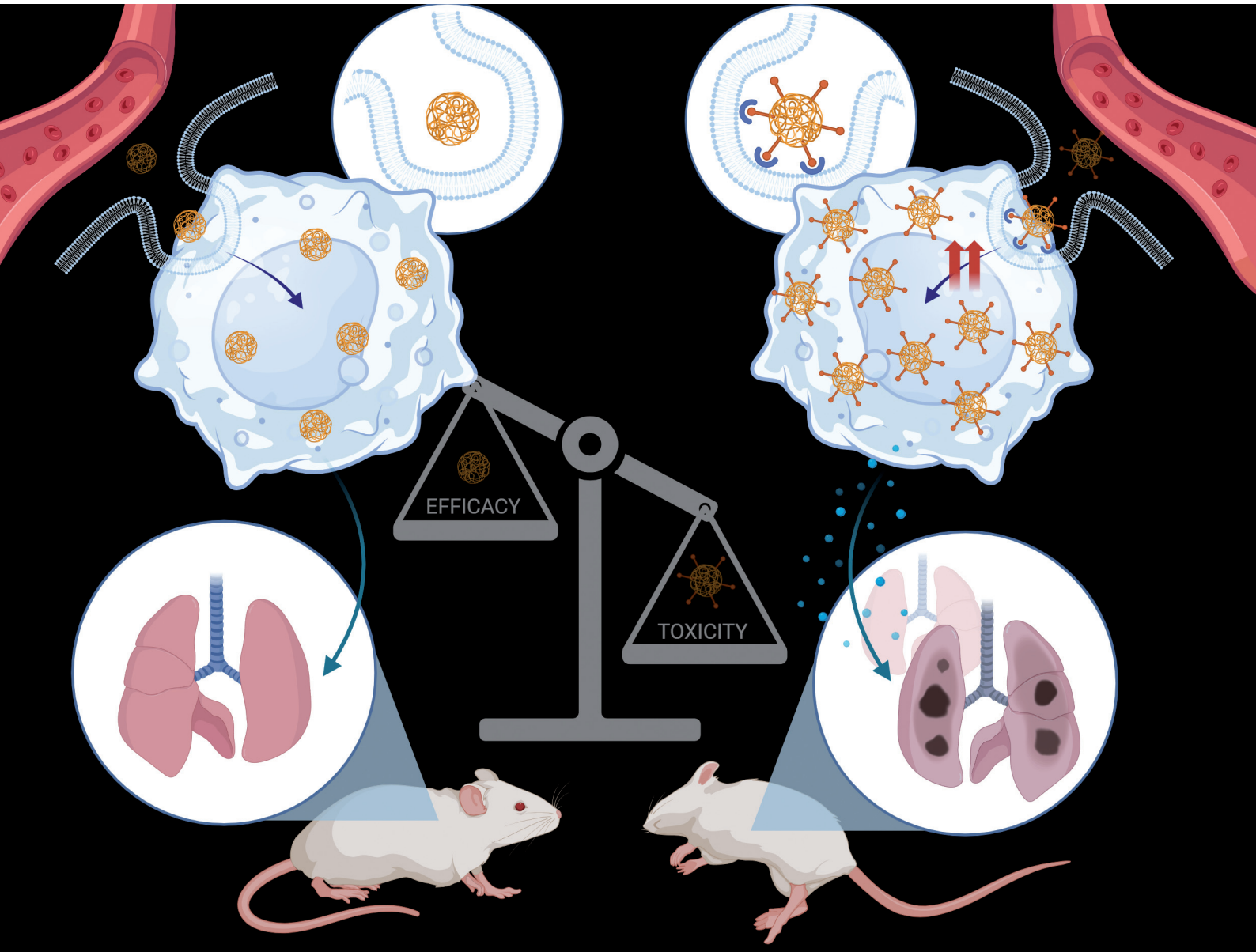


RSC Pharmaceutics

rsc.li/RSCPharma



eISSN 2976-8713



Cite this: *RSC Pharm.*, 2024, **1**, 430

Is receptor mediated active macrophage targeting of amphotericin B nanoformulations a promising approach?

Saugandha Das,^{†a} Pooja Todke,^{†a} Manisha Madkaikar^b and Padma Devarajan ^a

We present an AmB-LIPOMER anchored with Acemannan (ACEM), a mannose ligand for active macrophage targeting, *via* mannose receptor mediated endocytosis (RME). The AmB-LIPOMER prepared by modified nanoprecipitation was anchored with ACEM by simple incubation. FITC was added to obtain fluorescent LIPOMERs. The LIPOMERs revealed a spherical morphology, an average size of 400–450 nm and a PDI < 0.3. Reduction in the zeta potential and FTIR confirmed ACEM anchoring. Flow cytometry demonstrated a >13-fold enhancement of the FITC-ACEM LIPOMER *in vitro* in RAW 264.7 macrophage cells, compared to the FITC-LIPOMER, ascribed to mannose receptor mediated endocytosis. This was confirmed by the decreased uptake of the FITC-ACEM LIPOMER in the mannose receptor blocking study. Nevertheless, we were surprised by an ~2-fold decrease in the *in vitro* antileishmanial efficacy despite the augmented uptake of the ACEM LIPOMER. This poor efficacy was explained by the extensive localization of the FITC-ACEM LIPOMER in the lysosomal compartment, established by confocal microscopy, wherein AmB underwent rapid degradation. On the other hand phagocytic uptake and lipid mediated prolonged localization in the less harsh phagosome enabling lower degradation could have facilitated higher efficacy of the AmB-LIPOMER. The pharmacokinetic and biodistribution studies in rats revealed rapid and high reticuloendothelial system uptake. While the AmB-LIPOMER group exhibited no mortality, the mortality of 5 out of 6 animals in the AmB-ACEM LIPOMER group, within 15–30 minutes caused by lung necrosis was disturbing. While we propose an explanation for the toxicity, our study questions the rationale and safety of active targeting AmB using receptor mediated endocytosis.

Received 27th January 2024,
Accepted 2nd April 2024

DOI: 10.1039/d4pm00023d
rsc.li/RSCPharma

1. Introduction

Amphotericin B (AmB), which is a potent polyene macrolide antibiotic, is considered a drug of choice for visceral leishmaniasis (VL), a serious macrophage resident infection. Nevertheless, non-selective binding of AmB to host cells following intravenous administration has resulted in severe and near fatal renal toxicity with conventional AmB injection, leading to a need for safer and targeted alternatives.^{1,2}

Drug loaded nanocarriers, by mimicking the intracellular pathway of pathogens, have enabled high intracellular delivery of therapeutic payloads. Based on this premise, AmB loaded nanoformulations which rely on passive targeting approaches

have been developed to combine the advantages of high efficacy and low toxicity. Among nanoformulations, micellar formulations revealed significant toxicity, while liposomal AmB demonstrated both good efficacy and safety through macrophage targeted delivery, aided by the nanosize.³ Passive macrophage targeting of AmB was also achieved using different nanocarriers like solid lipid nanoparticles (SLNs),⁴ emulsomes,^{5,6} polymeric nanoparticles,^{7,8} nanodisks,⁹ and nanoemulsions.¹⁰ Our group has earlier reported macrophage targeted delivery of AmB-LIPOMERS by passive targeting. *In vitro* antileishmanial efficacy in amastigotes, was 2-fold higher and the safety index 3-fold higher compared to liposomal AmB.¹¹

Despite high effectiveness in the treatment of both leishmaniasis as well as a range of fungal infections, the dose-dependent kidney toxicity and systemic toxicity of AmB continue to pose serious concerns. Coupling targeted delivery with dose reduction strategies is one approach to tackle this challenge. In one study administration of oral AmB cochleates exhibited a dose-dependent reduction in mortality, a better therapeutic index with a survival rate of 70% and no compromise on efficacy.¹² Similarly, in another study, researchers demon-

^aDepartment of Pharmaceutical Sciences and Technology, Institute of Chemical Technology, Deemed University, Elite Status and Centre of Excellence (Maharashtra), N.P. Marg, Matunga (E), Mumbai, 400019 Maharashtra, India.

E-mail: pv.devarajan@ictmumbai.edu.in; Fax: +91 22 33611020;

Tel: +91 22 33612210

^bICMR-National Institute of Immunohaematology, KEM Hospital Campus, Parel, Mumbai, 400012 Maharashtra, India

†These authors contributed equally to this work.



stated that AmB cochleates protected *C. albicans* infected ICR mice following intraperitoneal administration at a low dose of $0.1 \text{ mg kg}^{-1} \text{ day}^{-1}$.¹³ In a mouse model of systemic candidiasis, AmB lipid nanospheres (1.0 mg kg^{-1}) demonstrated an enhanced survival rate and greater efficacy compared to AmBisome (8.0 mg kg^{-1}) or Fungizone (1.0 mg kg^{-1}).¹⁴ This served as the motivation to design an actively targeted AmB-LIPOMER to further augment intracellular uptake, in an attempt to decrease systemic toxicity and enable a possible reduction in dose without altering the efficacy.

Active targeting approaches can facilitate the delivery of significantly enhanced therapeutic cargoes inside the cell and have become an important focus area for the treatment of cancers and infectious diseases.¹⁵ Active targeting can improve uptake and thereby augment efficacy. For conditions like VL where the parasite *Leishmania donavani* is harboured safely inside macrophages, enhanced uptake through active targeting could provide a major advantage of improved efficacy,^{16,17} as well as the opportunity to decrease the dose, which could be very beneficial for drugs like AmB which exhibit high toxicity. Among various active targeting strategies, receptor mediated endocytosis is the most widely investigated and relies on ligands to target receptors overexpressed on cells.¹⁸ One such receptor overexpressed on macrophages where the leishmanial parasites are harboured is the mannose receptor, which exhibits high affinity for mannose and mannose-based macromolecules.¹⁹

Mannan conjugated to didanosine gelatin NPs exhibited a five-fold increase in intracellular macrophage uptake with augmented localization in lymph nodes, spleen, and the brain in the treatment of HIV.²⁰ A mannose-anchored thiolated AmB nanocarrier elicited a very high (71-fold) enhancement in intramacrophage drug uptake compared with the native drug.²¹ Furthermore, paramomycin loaded PLGA NPs coated with mannosylated thiolated chitosan demonstrated enhanced *in vitro* antileishmanial efficacy with a 36-fold lower IC₅₀ compared with the native drug. Moreover, the *in vivo* antileishmanial efficacy study indicated a 3.6-fold decreased parasitic burden in the *Leishmania donovani* infected BALB/c mice model.²² In another study, high intracellular delivery of rifampicin was achieved by surface modification of lipid NPs with chitosan-conjugated Acemannan (ACEM).²³

In the above studies the mannose-based ligands were attached by covalent conjugation of mannose to the nanocarrier, a major limitation being the complexity of synthesis.²⁴ Herein, we report for the first time ACEM as a mannose targeting ligand anchored to an AmB-LIPOMER by simple adsorption.

In an earlier study we reported a near two-fold enhancement in the *in vitro* efficacy of the AmB-LIPOMER in an antileishmanial amastigote model compared to the marketed liposomal formulation.¹¹ Based on the promise of further enhancement by active targeting, we embarked on designing a mannose receptor targeted AmB-LIPOMER using the known mannose ligand ACEM.^{25–27} The objective of the study was to confirm enhanced macrophage uptake in RAW 264.7 macro-

phage cells and enhanced efficacy in an *in vitro* antileishmanial amastigote model. Yet another objective was to evaluate the effect of ACEM anchoring on the pharmacokinetics and biodistribution of the AmB-LIPOMER in a rat model.

2. Materials and methods

2.1 Materials

AmB was a kind gift by Cipla Limited, Mumbai, India. Pluron Stearique WL1009 (polyglyceryl-6-distearate, PGDS) with a molecular weight (M_w) of $995.42 \text{ g mol}^{-1}$ was gifted by Gattefosse, France. Poly(methyl vinyl ether-*co*-maleic anhydride) and Gantrez® AN 119 (M_w : $872.78 \text{ g mol}^{-1}$) were provided by Ashland, Mumbai, India, while Trehalose 100 (M_w : $342.29 \text{ g mol}^{-1}$) was gifted by Gangwal Chemicals, Mumbai, India. Gift samples of Acemannan (ACEM) with $M_w \geq 1 \times 10^6$ Daltons and $\geq 20\%$ polymeric acetylated mannan content were provided by Naturaloe, Costa Rica. Magnesium acetate tetrahydrate pure, hydrochloric acid (35%) and potassium bromide were procured from Merck, Mumbai, India. Absolute ethanol (99.9% AR) was obtained from Changshu Hongsheng Fine Chemical Co., Ltd, China, while tetrahydrofuran (AR), isopropyl alcohol (HPLC grade), acetonitrile, methanol (HPLC grade), phenol and conc. sulphuric acid were obtained from Qualigens Thermo Fisher Scientific, India. Fetal bovine serum (FBS), Dulbecco's modified Eagle's medium (DMEM), antibiotic solution, 4',6-diamidino-2-phenylindole (DAPI; M_w : $350.25 \text{ g mol}^{-1}$), fluorescein isothiocyanate (FITC; M_w : $389.38 \text{ g mol}^{-1}$), dimethyl sulfoxide (cell culture grade) and MTT (3-[4,5-dicell methylthiazol-2-yl]2,5-diphenyltetrazolium bromide) with a M_w of $414.32 \text{ g mol}^{-1}$ were bought from HiMedia, Mumbai, India. Lysotracker™ Red and CellMask Deep Red were purchased from Thermo Fisher Scientific, India. Other analytical grade chemicals utilized for the study were procured as per use. The mouse monocyte macrophage cell line J-774A.1 was acquired from the National Centre for Cell Science, Pune, India.

2.2 Preparation of the ACEM anchored AmB-LIPOMER

Briefly, 20 mg of Gantrez AN119 (GZ) and 20 mg of AmB were solubilized in 6 ml of organic phase comprising an acidified mixture of tetrahydrofuran:ethanol (1:1) and was added under continuous magnetic stirring to a 30 ml aqueous phase consisting of 30% IPA in double distilled water. Furthermore, 40 mg of polyglyceryl-6-distearate (PGDS) solubilized in 2 ml of the above organic mixture was introduced into the aqueous phase which was followed by the addition of 3 ml, 5% w/v magnesium acetate. The AmB-LIPOMER dispersion was continuously stirred overnight for complete evaporation of the organic solvents. The solvent-free dispersion was centrifuged at 16 350g for 10 min resulting in separation of the AmB-LIPOMER pellet, while the supernatant was used for evaluation of the % drug entrapped. The pellet obtained was redispersed in filtered, double distilled water (5 ml) and disaggregated using an ultrasonic probe sonicator (DP120, Dakshin,



Mumbai, India) operating at 200 V with 10 s pulses for 5 min, to obtain the AmB-LIPOMER dispersion.

An aqueous solution of ACEM was prepared by dissolving the ligand in filtered, double distilled water at room temperature (28 °C), and vacuum filtered (0.2 µm filter), prior to use. The ACEM ligand solution was added to the resulting AmB-LIPOMER pellet at a GZ/ligand ratio of 1:1 (w/w), cyclo-mixed and allowed to stand for 10 min. The dispersion was probe sonicated for 5 min on an ice bath with 10 s pulses at 200 V, to obtain the AmB-ACEM LIPOMER.

The FITC loaded LIPOMER and ACEM-LIPOMER were prepared by the same method by replacing AmB with FITC (4 mg ml⁻¹).

2.3 Lyophilization study

AmB-LIPOMER and AmB-ACEM LIPOMER dispersions were lyophilized using a mixture of 10% Trehalose and 0.05% w/v Lutrol F68 as a cryoprotectant. The dispersions containing the cryoprotectant were dispensed into amber coloured glass vials. The vials were frozen for 24 h at -72 °C and lyophilized for another 24 h on a LABCONCO freeze dryer (FreeZone 4.5, USA). At the end of the cycle, the vials were tightly sealed with aluminium crimped rubber closures. The freeze-dried cake was reconstituted to an original volume (5 ml) with filtered double distilled water followed by shaking to obtain a homogeneous nanoparticle dispersion. The reconstituted formulations were further evaluated for particle size from which the S_f/S_i ratio was calculated.

2.4 ACEM anchored AmB-LIPOMER characterization

2.4.1 Entrapment efficiency. The nanoparticle supernatant was diluted with methanol AmB quantified at 405 nm by UV spectrophotometry (UV-1800 Spectrophotometer, Shimadzu, Japan). The % drug entrapped was calculated as follows:

$$\% \text{ Entrapment efficiency} = \frac{(\text{AmB}_{\text{total}} - \text{AmB}_{\text{supernatant}})}{\text{AmB}_{\text{total}}} \times 100$$

2.4.2 Drug loading. Accurately weighed quantities of the freeze-dried nanoparticles were solubilized in DMSO, followed by 15 min of cyclo-mixing and bath sonication. The samples were suitably diluted with methanol and % AmB loading was calculated using the equation below:

$$\% \text{ AmB loading} = \frac{(\text{Weight of AmB in NPs})}{(\text{Weight of NPs})} \times 100$$

2.4.3 Particle size and zeta potential. Briefly, the AmB-LIPOMER and the AmB-ACEM LIPOMER dispersed in filtered, double distilled water were diluted 100-fold and analysed in triplicate using a Nanobrook Series Brookhaven 90 plus PALS particle size analyzer (New York, USA). PS was measured at 25 °C at a scattering angle of 90°, while the zeta potential of the nanodispersions was determined by measuring electrophoretic mobility using electrophoretic light scattering (ELS) at a detection angle of 15°.

2.4.4 Transmission electron microscopy (TEM). Briefly, one drop each of the AmB-LIPOMER and the AmB-ACEM

LIPOMER dispersion was deposited onto a carbon grid (Ted Pella, Inc, Redding) and allowed to air dry. The nanoparticles were negatively stained with 1% phosphotungstic acid prior to analysis and analysed on a TECNAI 12 BT/FEI TEM at 120 kV.

2.4.5 Fourier transform infrared (FTIR) spectroscopy. The FTIR spectrum of AmB, excipients and the AmB-ACEM LIPOMER was performed on an FTIR (PerkinElmer, Spectrum Two, 10.4.2, USA). Each sample was blended with a suitable amount of KBr. The powders were then compressed on a hydraulic pellet press. Samples thus prepared were scanned in the region of 4000–650 cm⁻¹ to obtain the FTIR spectra.

2.4.6 Differential scanning calorimetry (DSC). Briefly, approx. 5–10 mg of each powder sample was added to individual aluminium pans and sealed. An empty aluminium pan served as a reference. The thermal behaviour of each sample was evaluated against the reference pan by heating the sealed aluminium pans from 40 to 300 °C at a heating rate of 10 °C min⁻¹ under a nitrogen atmosphere. DSC thermograms were recorded on a Pyris 6 DSC (PerkinElmer, Massachusetts, USA) using a previously reported method.

2.4.7 Powder X-ray diffraction. X-ray diffractograms of AmB, excipients, the AmB-LIPOMER and the AmB-ACEM LIPOMER were obtained using a Shimadzu 6100 diffractometer provided with Cu K α radiation ($\lambda = 1.54 \text{ \AA}$). XRD spectra were recorded at a voltage of 40 kV, a current of 40 mA, a scanning speed of 2 θ min⁻¹ and scanning angles from 5° to 50° (2 θ), with a step size of 0.02.

2.5 Stability study

Stability was evaluated over a duration of 12 months at 4 ± 2 °C and 25 ± 2 °C/60 ± 5% RH according to the ICH guidelines. The lyophilized AmB-LIPOMER and AmB-ACEM LIPOMER were stored in amber coloured glass vials (10 ml) with rubber stoppers and aluminium-crimped tops. Samples were removed from the stability chambers at fixed time intervals of 0, 1, 2, 3, 6 and 12 months and various parameters, like visual examination, PS, and PDI, were evaluated in triplicate as described in section 2.4.3 while the drug content was evaluated as described below.

The AmB content was estimated by reverse phase HPLC using a Jasco LC 2000 (Jasco, Japan), fitted with a PDA detector. Sample analysis was performed under isocratic elution conditions, using a C18 Waters column (250 × 4.6 mm, 5 µm PS) at a temperature of 25 °C. The mobile phase comprising 50 mM disodium EDTA : acetonitrile (55 : 45) was maintained at a flow rate of 1.2 ml min⁻¹. For sample preparation, the freeze-dried AmB-LIPOMER and AmB-ACEM LIPOMER were accurately weighed and transferred into DMSO and allowed to dissolve by cyclo-mixing and bath sonication for 15 min, followed by suitable dilution with methanol. The concentration of AmB was quantified in triplicate at a λ_{max} of 405 nm by RP-HPLC.

2.6 *In vitro* serum stability of nanoparticles

Briefly, 0.5 ml each of the AmB-LIPOMER and the AmB-ACEM LIPOMER dispersions (~2 mg ml⁻¹ AmB) were incubated with



an equal volume of rat serum maintained at 37 ± 0.5 °C. Aliquots of 0.1 ml were withdrawn at time intervals of 1, 2, 4, and 6 h, diluted 100-fold with filtered, double distilled water and evaluated for alteration in PS in triplicate as detailed in section 2.4.3.

2.7 Macrophage cell viability

The RAW 264.7 macrophage cell line was maintained as reported previously. RAW 264.7 cells grown in 10% FBS supplemented DMEM medium were seeded in a 96-well plate, containing 5000 cells per well. The well plates were incubated overnight, at 37 °C with a supply of 5% CO₂ for cell adherence. Serial dilutions of the blank LIPOMER, the blank ACEM LIPOMER, the AmB-LIPOMER and the AmB-ACEM LIPOMER were prepared in complete medium to acquire varying AmB concentrations from 1.56 to 50 µg ml⁻¹, which were added to the wells in triplicate. Plain medium treated cells were used as the control. The well plates were incubated for 24 h at 37 °C, after which the test solutions were discarded. This was followed by the addition of 100 µL of MTT solution (500 µg ml⁻¹) in each well and incubation for another 4 h to result in the formation of purple coloured formazan crystals. The MTT solution was aspirated and the formazan crystals were dissolved in DMSO (200 µL). The absorbance of the wells was recorded at 570 nm employing a multi-well microplate reader (BIO-TEK, Plate reader, Germany) and % cell viability was evaluated as described in the equation below:

$$\% \text{ Macrophage cell viability} = \frac{(\text{Absorbance}_{\text{sample}})}{\text{Absorbance}_{\text{control}}} \times 100$$

2.8 Macrophage uptake

2.8.1 Flow cytometry. RAW 264.7 macrophage cells (1×10^5 cells per well) were allowed to adhere after seeding in a 24-well plate for 24 hours. At the end of 24 h, the medium was discarded followed by incubation of cells with the FITC loaded LIPOMER (FITC-LIPOMER), the ACEM anchored LIPOMER (FITC-ACEM-LIPOMER) (equivalent to 25 µg ml⁻¹) and medium as the control for up to 24 h. At 15 min, 1 h, 4 h and 24 h the cells were dislodged by trypsinization and the resulting cell suspensions were pipetted out into flow tubes and centrifuged for 5 min at 1008g and at a low temperature (4 °C). The pellet obtained was washed with PBS and the process was repeated three times to wash off the free FITC on the surface of the cells. The cells were resuspended in PBS and analysed at λ_{EX} (485 nm) and λ_{EM} (538 nm) using a fluorescence activated cell sorter (FACSCalibur flowcytometer, BD BioSciences, USA). The cells were gated according to forward scatter *versus* side scatter and data were analysed using FlowJo software (Treestar).

2.8.2 Mannose blocking study by confocal microscopy. RAW 264.7 macrophage cells (1×10^5 cells per well) containing the FITC-LIPOMER and the ACEM-LIPOMER (25 µg ml⁻¹) in fresh medium were incubated at 37 °C for 1 h. For the blocking experiment, the cells were incubated with free D-mannose (500 µM) for 1 h, and then transferred into fresh medium containing the FITC-ACEM-LIPOMER for 2 h. The cells were washed three times in PBS and fixed with 4% paraformalde-

hyde. Cell nuclei were counterstained with DAPI (300 nM) for 20 min. The cells were washed three times with PBS and incubated with the lysosome specific dye Lysotracker™ Red (75 nM) for 30 min. Furthermore, the cells were again washed three times with PBS and incubated with the cell membrane specific dye CellMask Deep Red (250 nM) for 10 min. Intramacrophage uptake and intracellular localization were visualized using a laser scanning confocal microscope, followed by analysis of images using ImageJ version 2.0.0 software.²⁸

2.9 *In vitro* anti-leishmanial efficacy

Nanoparticle mediated growth inhibition of transgenic *Leishmania donovani* amastigote infected J774A.1 macrophage cells was evaluated using a previously reported method.¹¹ Varying dilutions of the AmB-LIPOMER and the AmB-ACEM LIPOMER were prepared in DMEM complete medium to obtain AmB concentrations from 2.5 to 50 ng ml⁻¹. The samples were added to the amastigote (2.5×10^5 per well) infected macrophage cells (5×10^4 cells per well) seeded on a 96-well plate and incubated for 72 h at 37 °C. At the end of 72 h, the samples from each well were discarded and replaced with 50 µL each of Steady-Glo reagent and PBS, and gently mixed for 1–2 min. The luciferase activity of each well was measured in terms of the relative luminescence unit (RLU) and parasitic growth inhibition was calculated using the equation:

$$\% \text{ Amastigote inhibition} = \frac{(\text{RLU}_{\text{control}} - \text{RLU}_{\text{treated}})}{\text{RLU}_{\text{control}}} \times 100$$

2.10 Safety evaluation

The safety of the AmB-ACEM LIPOMER was evaluated *via* hemolysis assay. Briefly, varying dilutions of the AmB-LIPOMER, the AmB-ACEM LIPOMER and commercial AmB formulations (Amfocare® and Fungisome™) were prepared in 5% v/v dextrose solution to obtain AmB concentrations from 50 to 1000 µg ml⁻¹. Each sample was added to an erythrocyte suspension of 5% v/v and incubated at 37 °C for 1 h. At the end of 1 h the sample tubes were immersed in ice cold water to halt the process and the intact erythrocytes were separated by centrifuging for 15 min at 1008g. The supernatant was analysed for released hemoglobin by measuring absorbance at 540 nm. Hemolysis observed was compared against the negative control (PBS) and the positive control (deionized water), and percentage hemolysis was calculated employing the equation:

$$\% \text{ Hemolysis} = \frac{(\text{Absorbance}_{\text{sample}} - \text{Absorbance}_{\text{PBS}})}{(\text{Absorbance}_{\text{water}} - \text{Absorbance}_{\text{PBS}})} \times 100$$

2.11 *In vivo* pharmacokinetics and biodistribution

The study protocol was approved by the Institutional Animal Ethics Committee (IEAC) of the Institute of Chemical Technology, Mumbai, India, in accordance with the CPCSEA guidelines (protocol no.: ICT/IAEC/2018/P13). Male Sprague-Dawley (SD) rats (250 ± 20 g) were quarantined in the animal house of the Institute of Chemical Technology, Mumbai,



India, under controlled temperature and humidity ($25^{\circ}\text{C} \pm 2^{\circ}\text{C}$, $50 \pm 5\%$ RH) with a 12 h dark/light cycle throughout the study.

2.11.1 Pharmacokinetics. Animals were divided into one untreated control group of two animals and three treatment groups of six animals each *viz.* the AmB-LIPOMER, the AmB-ACEM LIPOMER and FungisomeTM groups. Lyophilized AmB-NPs and FungisomeTM were diluted with 5% dextrose and were administered i.v. *via* the tail vein at a dose equivalent to 5 mg kg⁻¹ AmB. The animals were anesthetized (using gaseous isoflurane) and blood samples (0.5 mL) were collected into anticoagulant containing centrifuge tubes (20 μL EDTA per mL of blood) at 0, 0.083, 0.25, 0.5, 1, 4, 8, 12 and 24 and 48 h post-dosing by retro-orbital puncture. Plasma was separated by centrifugation at 4000g for 10 min at 4 °C and samples were stored at -80 °C to avoid drug degradation until analysis. On the day of analysis, the plasma samples were deproteinized using methanol and the centrifuged supernatant was quantified using the reverse phase HPLC method with a PDA detector at 405 nm using Erlotinib (IS). Various pharmacokinetic parameters were analysed with a non-compartmental model using Phoenix WinNonlin software version 6.3.

2.11.2 Biodistribution. Rats were divided into one untreated control group of two animals and three treatment groups of fifteen animals each *viz.* the AmB-LIPOMER, the AmB-ACEM LIPOMER and FungisomeTM groups. Lyophilized AmB NPs and FungisomeTM were diluted with 5% dextrose and were administered i.v. *via* the tail vein at a dose equivalent to 5 mg kg⁻¹ AmB. Rats were sacrificed using excess carbon dioxide and dissected at 30 min, 4 h, 12 h, 24 h, and 48 h post-dosing. Major organs such as the liver, spleen, heart, kidneys and lungs were harvested, washed in normal saline and packed individually into labelled zip lock bags which were immediately stored at -80 °C to avoid drug degradation until analysis. On the day of analysis, the organs were thawed and homogenized, an aliquot was deproteinized using methanol and the centrifuged supernatant was quantified using the reverse phase HPLC method with a PDA detector at 405 nm using Erlotinib (IS). The results for each organ were presented as the concentration of AmB per gram of tissue *versus* the time point.

The overall targeting efficiency of AmB-SLN and the LIPOMER was calculated using the equation:

$$\text{Targeting efficiency (\%)} = \frac{\sum_{i=1}^n (\text{AUC}_{0-\infty})_i}{\sum_{i=1}^n (\text{AUC}_{0-\infty})_i} \times 100$$

where the numerator refers to AmB exposure to RES organs and the denominator refers to the sum total of AmB exposure to all the tissues, including the target tissue ($\text{AUC}_{0-\infty}$)_i.

2.12 Statistical analysis

All studies were carried out in triplicate and the mean \pm standard deviation of the three independent experiments was calculated. Statistical analysis was carried out using one-way

ANOVA with Tukey's test and a *P*-value of <0.05 was selected to indicate statistical significance. The IC_{50} value was calculated by regression of log dose *versus* drug response obtained through probing analysis.

3. Results and discussion

3.1 ACEM anchored AmB-LIPOMER

The AmB-LIPOMER was prepared using a method previously reported by our group.¹¹ The characteristic frequencies of ACEM in the fingerprint region corresponding to the C–O pyranose ring and C–O–C ether groups (<1400 cm⁻¹) remained intact.^{29,30} However, the sharp bands at 1852.17, 1779.86, and 1725.61 cm⁻¹, characteristic of anhydride lactone of GZ and at 3400 cm⁻¹ and 1740 cm⁻¹ corresponding to the O–H stretching vibrations and C=O stretching vibrations of ACEM, respectively, were absent in the FTIR spectrum of the AmB-ACEM LIPOMER indicating H-bonding interactions between ACEM and GZ (Fig. 1), which aided noncovalent anchoring of ACEM.

The AmB-LIPOMER and the AmB-ACEM LIPOMER demonstrated high AmB entrapment efficiencies of $97.76 \pm 0.56\%$ and $95.51 \pm 0.04\%$ and drug loadings of $21.58 \pm 0.39\%$ and $21.16 \pm 0.55\%$. A negative zeta potential (-14.78 ± 0.92 mV and -19.65 ± 0.89 mV), respectively, indicated good colloidal stability. A mean diameter in the range of 300–450 nm with a low PDI (<0.3) is considered apposite for intramacrophage targeting. Lyophilization of the AmB-LIPOMER and the AmB-ACEM LIPOMER to ensure long-term stability revealed S_f/S_i ratios of 1.24 ± 0.16 and 1.21 ± 0.02 , respectively.

3.2 Imaging by TEM

TEM images of the AmB loaded nanocarriers revealed a nearly spherical morphology with the particle size correlating with those reported by DLS measurements (Fig. 2).

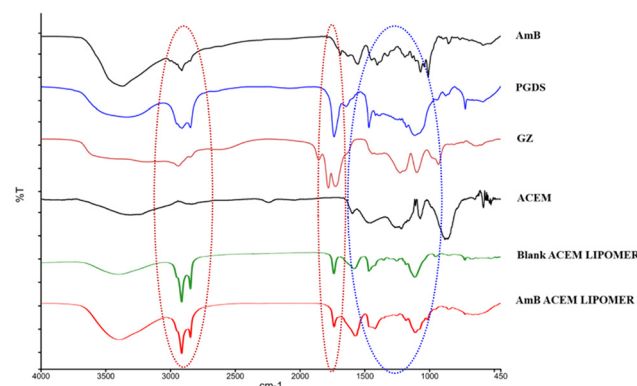


Fig. 1 FTIR spectra of AmB, GZ, PGDS, ACEM and AmB-ACEM LIPOMER. The blue dotted circle represents the characteristic frequencies of ACEM in the fingerprint region that remained intact, thereby confirming anchoring of ACEM. Red dotted circles represent the AmB-ACEM LIPOMER indicating H-bonding between ACEM and GZ.



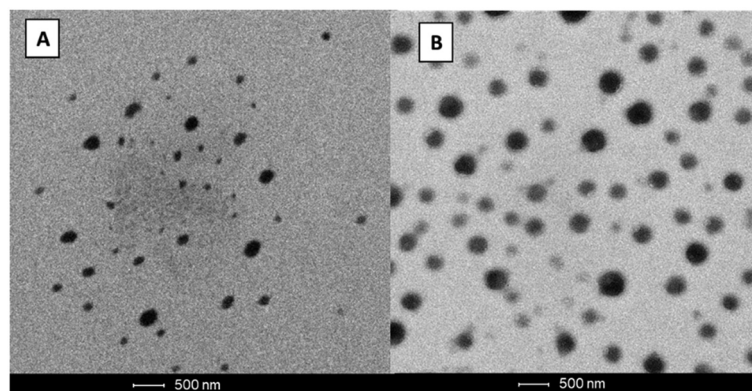


Fig. 2 Transmission electron microscopy analysis of (A) the AmB-LIPOMER and (B) the AmB-ACEM LIPOMER.

3.3 DSC and XRD analyses

DSC thermograms (Fig. 3A) revealed two broad endothermic peaks at 115.63 °C and 202.64 °C for AmB, which corroborated earlier reports.^{31,32} The disappearance of these characteristic peaks in the AmB-ACEM LIPOMER suggests decreased crystallinity and partial amorphization of AmB in the NPs. Such a decrease indicates enhanced dissolution.³³

XRD analysis has been used for quantifying the extent of the amorphous or crystalline phase in nanosolids. In agreement with previous reports^{34,35} AmB demonstrated multiple sharp endothermic peaks at 2θ scattered angles between 10 and 24° indicating a high degree of crystallinity. PGDS also exhibited a sharp peak at a 2θ value of 22° while GZ and ACEM indicated a relatively amorphous state. The absence of the sharp drug and lipid peaks in the AmB-ACEM LIPOMER (Fig. 3B) indicated partial amorphization of the drug in the nanoparticles.

3.4 Long-term stability study

The freeze dried AmB-LIPOMER and AmB-ACEM LIPOMER revealed a drug content of >94% and no significant change in physical appearance or particle size (Fig. 4) over a period of

12 months under refrigerated conditions confirming good stability as per ICH guidelines.

3.5 Serum stability

Protein binding has been posited as one of the key factors influencing particle internalization. Serum proteins, particularly opsonins which are adsorbed on the surface of nanocarriers, tag them for recognition and clearance by the macrophages of the RES.³⁶ Such adsorption leads to alterations in the size of nanocarriers. The LIPOMERs were stable up to 6 h revealing no significant increase in the particle size and an average size not exceeding 500 nm, indicating safety for i.v. administration (Fig. 5). The stability of the LIPOMERs is credited to surface hydrophilicity induced steric stabilization imparted by GZ and ACEM.³⁷

3.6 Hemolysis assay

Hemolytic activity is a well-known toxicity associated with AmB. Different marketed formulations served as controls in this study. The conventional micellar AmB, Amphocare®, reported to be toxic, revealed ~100% hemolysis even at low AmB concentrations (Fig. 6). This is ascribed to the rapid dissociation of AmB from deoxycholate micelles into the aggre-

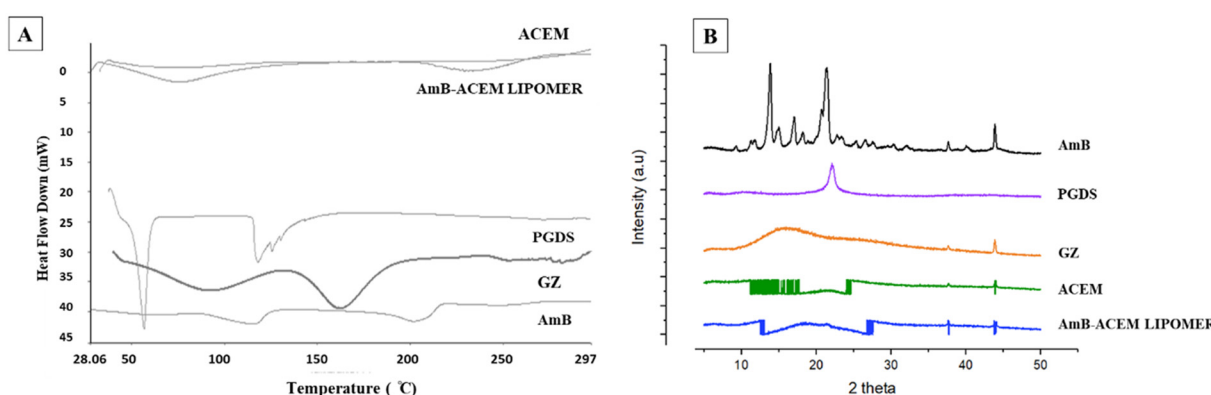


Fig. 3 (A). DSC thermograms of AmB, GZ, PGDS, ACEM and the AmB-ACEM LIPOMER. (B) XRD spectra of AmB, GZ, PGDS, ACEM, and the AmB-ACEM LIPOMER.



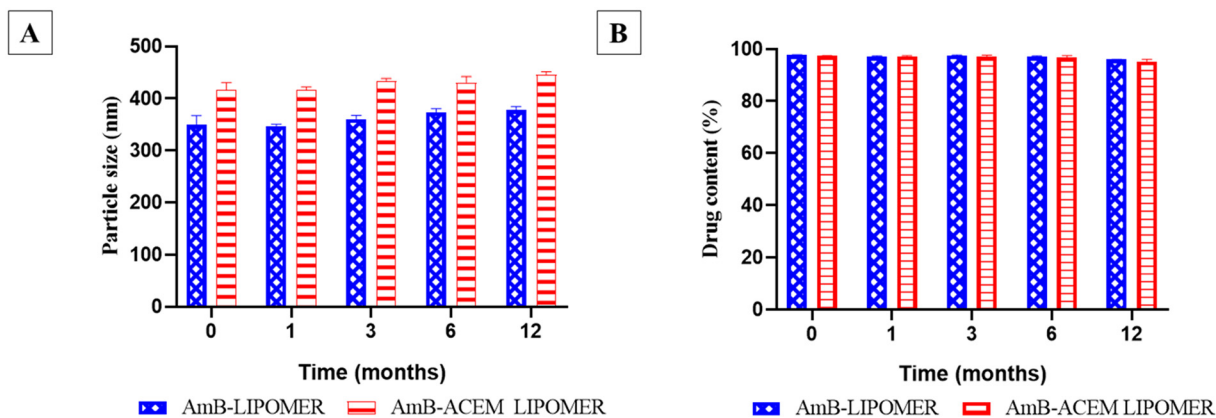


Fig. 4 Long term stability study of the AmB-ACEM LIPOMER and the AmB-LIPOMER: (A) particle size (nm) and (B). drug content (%). Data are presented as mean \pm SD, $n = 3$.

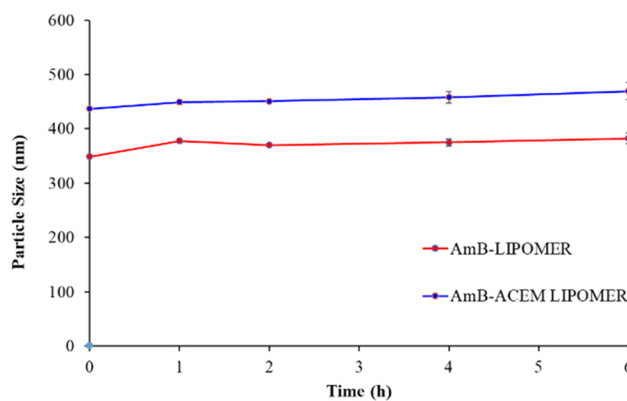


Fig. 5 Serum stability study of the AmB-ACEM LIPOMER and the AmB-LIPOMER. Data are presented as mean \pm SD, $n = 3$.

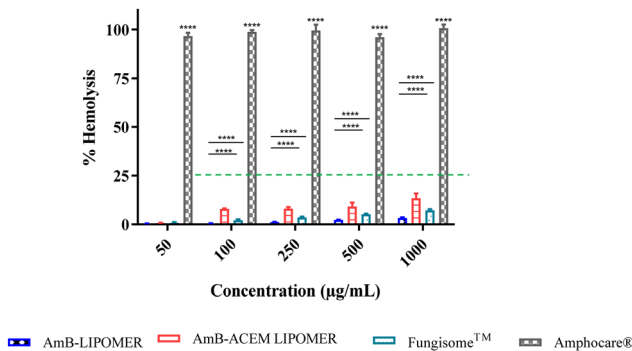


Fig. 6 Erythrocyte toxicity of the AmB-ACEM LIPOMER and the AmB-LIPOMER, in comparison with Amphocare® and Fungisome™ diluted in 5% dextrose to obtain varying AmB concentrations, after 1 h of incubation. Data are presented as mean \pm SD, $n = 3$, at a significance level of $****p < 0.0001$.

gated state upon dilution, which is heightened by the hemolytic activity of the surfactant in Amphocare®.³⁸ On the other hand, the AmB-ACEM LIPOMER revealed less than 15% hemolysis even at high AmB concentrations (Fig. 6), comparable with the AmB-LIPOMER and Liposomal AmB (Fungisome™), endorsing safety for i.v. administration.³⁹

lysing even at high AmB concentrations (Fig. 6), comparable with the AmB-LIPOMER and Liposomal AmB (Fungisome™), endorsing safety for i.v. administration.³⁹

3.7 Macrophage cell viability

The AmB-ACEM LIPOMER revealed good safety, as even at a high AmB concentration of $50 \mu\text{g ml}^{-1}$, $>71\%$ cell viability was achieved (Fig. 7). The blank AmB-LIPOMER and the AmB-LIPOMER revealed near 100% cell viability suggesting good safety while the blank ACEM LIPOMER demonstrated high cell proliferation.

3.8 Macrophage uptake study

Based on the macrophage viability data, the AmB concentration equivalent to $25 \mu\text{g ml}^{-1}$ (~80% cell viability) was selected for the macrophage uptake study. A 13- to 20-fold enhancement in the fluorescence intensity was observed with the FITC loaded ACEM LIPOMER compared to the LIPOMER

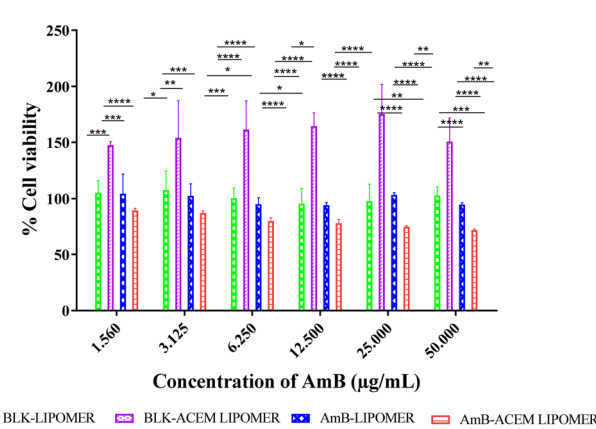


Fig. 7 Concentration dependent cytotoxicity of the blank LIPOMER, blank ACEM LIPOMER, AmB-LIPOMER, and AmB-ACEM LIPOMER against the RAW 264.7 cell line after 24 h of incubation. Data are presented as mean \pm SD, $n = 3$, at significance levels of $*p < 0.05$, $**p < 0.01$, $***p < 0.001$, and $****p < 0.0001$.



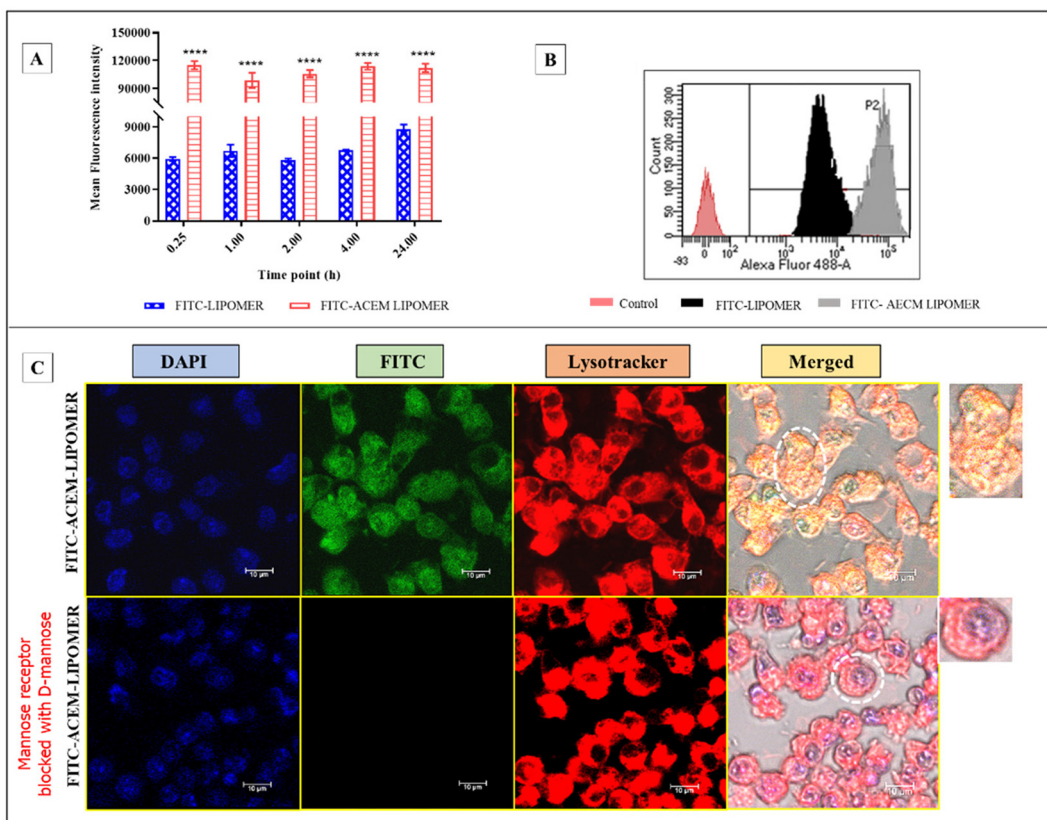


Fig. 8 Macrophage uptake study of the FITC-LIPOMER and the ACEM LIPOMER (A). Uptake by flow cytometry – change in the mean fluorescence intensity with time. (B). Overlay graph of fluorescence intensity. Data are presented as mean \pm SD, $n = 3$, at a significance level of *** $p < 0.0001$. (C). Uptake by confocal microscopy – fluorescence intensity in macrophages with FITC-ACEM-LIPOMER + D-mannose and the FITC-ACEM-LIPOMER, respectively; scale bar, 10 μ m.

at all time points (Fig. 8A and B). The high macrophage uptake confirmed the role of ligand based active targeting in enabling augmented macrophage uptake, and corroborated other reports on carbohydrate enabled mannose receptor mediated uptake.^{40–42} Nevertheless, we confirmed the same by performing the mannose receptor blocking assay, aided by confocal microscopy. A significant reduction in uptake of the FITC-ACEM LIPOMER in mannose treated macrophages validated the mannose receptor mediated uptake facilitated by ACEM. Furthermore, the yellow fluorescence seen due to integration of the green fluorescence of FITC with the lysotracker red dye also suggested high lysosomal localization of the FITC-ACEM LIPOMER. This could be particularly advantageous in enabling high efficacy in leishmaniasis, wherein the parasite is harboured in the lysosome.⁴³

3.9 Anti-leishmanial efficacy

The data demonstrate comparable efficacy of the AmB-ACEM LIPOMER with that of liposomal AmB (FungisomeTM) which served as the reference (Table 1). Surprisingly the AmB-LIPOMER without ACEM, despite a lower macrophage uptake, revealed a 2-fold lower IC₅₀ value and higher efficacy compared to both liposomal AmB and the AmB-ACEM LIPOMER. The AmB-LIPOMER also demonstrated a signifi-

Table 1 Comparison of *in vitro* anti-leishmanial efficacy and safety of the AmB-LIPOMER, the AmB-ACEM LIPOMER and FungisomeTM; data are expressed as mean \pm SD ($n = 3$)

Formulation	IC ₅₀ (ng mL ⁻¹) amastigote	CC ₅₀ (ng mL ⁻¹)	SI
AmB-LIPOMER	7.55 \pm 1.16	556.66 \pm 15.45	73.72
AmB-ACEM LIPOMER	14.45 \pm 0.31	198.83 \pm 20.67	13.75
Fungisome TM (Liposomal AmB)	13.55 \pm 0.91	333.83 \pm 29.00	24.63

cantly higher safety index compared to the AmB-ACEM LIPOMER as well as liposomal AmB.

The lower efficacy is ascribed to the receptor mediated endocytic uptake of the ACEM-LIPOMER and the extensive localization of the AmB-ACEM LIPOMER resulting in the lysosomal compartment as substantiated by the confocal images (Fig. 8C). Rapid degradation of AmB in the harsh and acidic lysosomal pH^{44,45} resulted in decreased efficacy. The AmB LIPOMER exhibited phagocytic uptake in the absence of the ligand and localisation in the phagosome. Possible delay in phagosomes maturation due to the lipidic nature of the carrier as reported in other studies^{46–48} resulting in delay in phagoly-



sosomal fusion could have limited the degradation of AmB, thereby enabling higher efficacy.

3.10 Pharmacokinetics and biodistribution study

The plasma profile after intravenous administration of the AmB-LIPOMER and liposomal FungisomeTM demonstrated rapid clearance from the plasma, possibly by the macrophages (Fig. 9). Furthermore, the pharmacokinetic profile of the AmB-LIPOMER and FungisomeTM demonstrated similar areas under the curve (AUC) and extensive tissue distribution was indicated by the high volume of distribution ($V_d > 7$ L). Although the AmB-LIPOMER exhibited a 1.43-fold lower plasma half-life compared to liposomal FungisomeTM, it presented a 1.57-fold higher mean residence time (MRT), respectively, compared to FungisomeTM, indicating longer retention in the body (Table 2).

In the case of the AmB-ACEM LIPOMER, rapid plasma clearance was evident following intravenous administration, as at 5 minutes the plasma concentration was very low ($0.36 \pm 0.09 \mu\text{g mL}^{-1}$). This was 25.61-fold and 81-fold lower compared to the AmB-LIPOMER and FungisomeTM, respectively, suggesting very rapid distribution into the RES organs. Overall

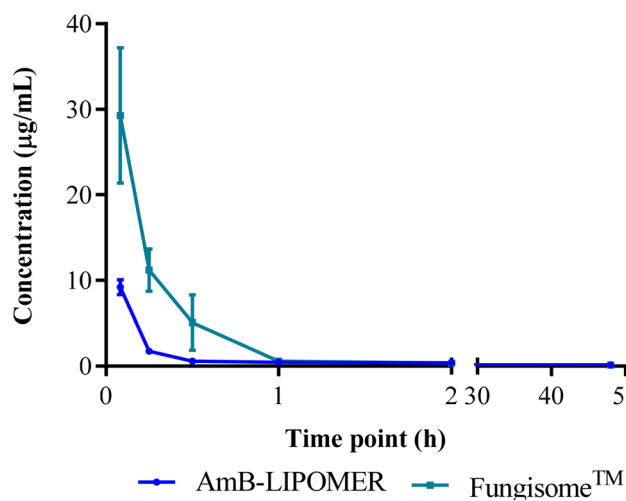


Fig. 9 Pharmacokinetic profile of AmB after intravenous administration of the AmB-LIPOMER and FungisomeTM at 5 mg kg^{-1} dose ($n = 3$).

Table 2 Pharmacokinetic parameters of AmB after intravenous administration of the AmB-LIPOMER and FungisomeTM in rats at 5 mg kg^{-1} dose ($n = 3$)

Pharmacokinetic parameters	Treatment groups (5 mg kg^{-1})	
	AmB-LIPOMER	Fungisome TM
C_0 ($\mu\text{g mL}^{-1}$)	21.57 ± 4.87	56.45 ± 11.42
$t_{1/2}$ (h)	31.89 ± 9.04	45.63 ± 5.87
AUC_{0-t} ($\text{h } \mu\text{g mL}^{-1}$)	12.41 ± 1.06	17.96 ± 2.13
V_d (L kg^{-1})	10.94 ± 2.31	7.87 ± 2.11
C_1 ($\text{mL h}^{-1} \text{ kg}^{-1}$)	0.27 ± 0.05	0.20 ± 0.02
MRT_{0-t} (h)	14.95 ± 1.23	9.12 ± 2.32

however, while the AmB-ACEM LIPOMER dosed animal revealed an RES targeting efficiency of $\sim 84\%$, the AmB-LIPOMER and FungisomeTM demonstrated RES targeting efficiencies of $> 92\%$. The AmB-LIPOMER and FungisomeTM revealed high localization in the clinically relevant VL reservoirs, namely the liver and spleen, with significantly lower amounts in the non-target organ, lungs (Fig. 10A). In the case of the AmB-ACEM LIPOMER, within 30 min 5 of the 6 animals exhibited severe respiratory distress, laboured breathing, difficulty in movement, leg twitching and death due to asphyxiation. The AmB-ACEM LIPOMER group revealed enhanced concentration not only in the liver, but also in the lungs, kidneys and heart (Fig. 10A). Furthermore, gross examination of the organs of the deceased animals revealed a significant increase in the size of the lungs, with severe inflammation, congestion and clotting compared to the lungs of AmB-LIPOMER treated animals (Fig. 10B). Neither the AmB-LIPOMER nor FungisomeTM groups showed such adverse effects and mortality.

Pulmonary accumulation and adverse reactions have been reported in humans, shortly after administration of commercial liposomal AmB, but only in patients with liver damage. The reduced liver clearance of liposomal AmB in such patients consequently enhanced the deposition of liposomes in the lungs, which act as a substitutive clearing organ.^{49–51}

Extrapolating this to our study, the extremely rapid uptake and high concentration of the AmB-ACEM LIPOMER probably resulted in saturation of the liver macrophage receptors supported by the rapid distribution observed in the pharmacokinetic study. This resulted in significantly enhanced deposition in the lungs, the substitutive clearing organ, causing severe

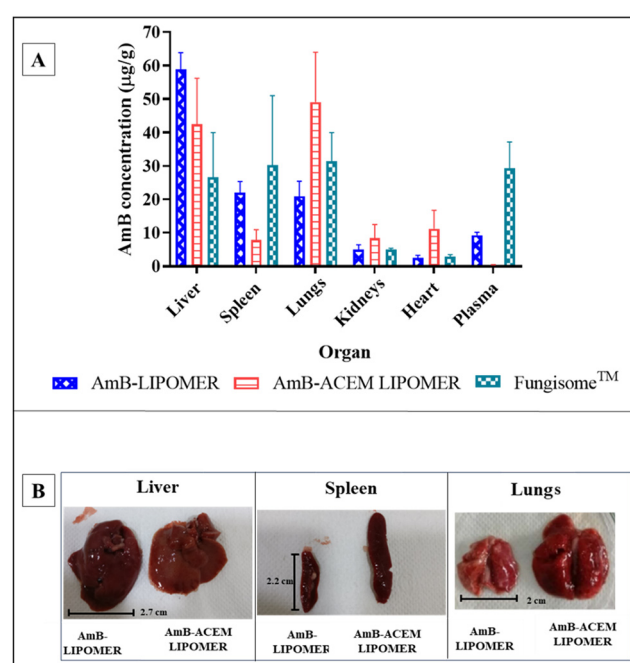


Fig. 10 (A) Biodistribution of the AmB-LIPOMER, the AmB-ACEM LIPOMER and FungisomeTM, mean \pm SD ($n = 3$); (B) liver, spleen and lungs of the AmB-LIPOMER and the AmB-ACEM LIPOMER dosed rats (<30 minutes) after intravenous administration at a 5 mg kg^{-1} dose.



inflammation and subsequent mortality (Fig. 10B). Moreover, complex carbohydrates like ACEM act as immune stimulators of both macrophages and T cells which can trigger enhanced macrophage/mononuclear cell infiltration and stimulate the production of proinflammatory agents (cytokines, tumour necrosis factor and nitric oxide) resulting in untoward effects as observed in our study,²⁶ although another report suggests that ACEM could inhibit the cytokine storm in mouse pneumonia.⁵² Furthermore, pulmonary hypertension and lung damage caused by AmB have also been reported,⁵³ which have been associated with enhanced immune cell aggregation and the production of chemical mediators by macrophages. This could have further aggravated the condition.

This brings to the forefront a serious concern about the strategy of active targeting of AmB, even though the safety of ACEM, a carbohydrate ligand, has been demonstrated. The study also highlights the need for a rational approach to titrating the augmented intracellular drug concentration, particularly for toxic drugs like AmB.

4. Conclusion

Active targeting using a mannose receptor-based ligand is a promising approach for manifold enhancement in the intracellular delivery of drugs. Nevertheless, this study proposes caution in active macrophage targeting of AmB, as the high mannose receptor uptake proved seriously detrimental instead of being advantageous. Our study also demonstrated the AmB-LIPOMER without the ACEM ligand to be comparable with the gold standard liposomal AmB, proposing passive targeting as the safer option.

Author contributions

Saugandha Das: conceptualization, methodology, investigation, software, and writing – original draft. Pooja Todke: conceptualization, methodology, investigation, software, and writing – original draft. Manisha Madkaikar: methodology, investigation, and validation. Padma Devarajan: conceptualization, investigation, supervision, validation, funding acquisition, and manuscript – reviewing and editing.

Conflicts of interest

There are no conflicts to declare.

Acknowledgements

The present research was supported by the Department of Science and Technology (DST) under the INSPIRE fellowship scheme (INSPIRE Fellowship Code No. IF130037), Government of India, New Delhi (India). The authors are thankful to the All India Council for Technical Education (AICTE), Government of

India, and TEQIP-III for providing research fellowship to Pooja Todke (Student ID: 1-6431958581).

References

- 1 M. Baginski, J. Czub and K. Sternal, *Chem. Rec.*, 2006, **6**, 320–332.
- 2 V. Fanos and L. Cataldi, *J. Chemother.*, 2000, **12**, 463–470.
- 3 B. L. Burgess, Y. He, M. M. Baker, B. Luo, S. F. Carroll, T. M. Forte and M. N. Oda, *Int. J. Nanomed.*, 2013, 4733–4743.
- 4 S. Gupta, A. Dube and P. Vyas, *Pharm. Nanotechnol.*, 2012, **1**, 54–67.
- 5 S. Gupta and S. P. Vyas, *J. Drug Targeting*, 2007, **15**, 206–217.
- 6 S. Gupta, A. Dube and S. P. Vyas, *J. Drug Targeting*, 2007, **15**, 437–444.
- 7 M. Nahar and N. K. Jain, *Pharm. Res.*, 2009, **26**, 2588–2598.
- 8 R. Kumar, G. C. Sahoo, K. Pandey, V. N. Das and P. Das, *Drug Delivery*, 2015, **22**, 383–388.
- 9 K. G. Nelson, J. V. Bishop, R. O. Ryan and R. Titus, *Antimicrob. Agents Chemother.*, 2006, **50**, 1238–1244.
- 10 S. Asthana, A. K. Jaiswal, P. K. Gupta, V. K. Pawar, A. Dube and M. K. Chousaria, *Antimicrob. Agents Chemother.*, 2013, **57**, 1714–1722.
- 11 S. Das and P. V. Devarajan, *Mol. Pharm.*, 2020, **17**, 2186–2195.
- 12 G. Delmas, S. Park, Z. W. Chen, F. Tan, R. Kashiwazaki, L. Zarif and D. S. Perlin, *Antimicrob. Agents Chemother.*, 2002, **46**, 2704–2707.
- 13 L. Zarif, J. R. Graybill, D. Perlin, L. Najvar, R. Bocanegra and R. J. Mannino, *Antimicrob. Agents Chemother.*, 2000, **44**, 1463–1469.
- 14 H. Fukui, T. Koike, T. Nakagawa, A. Saheki, S. Sonoke, Y. Tomii and J. Seki, *Int. J. Pharm.*, 2003, **267**, 101–112.
- 15 A. Jhaveri and V. Torchilin, *Expert Opin. Drug Delivery*, 2016, **13**, 49–70.
- 16 N. K. Jain, V. Mishra and N. K. Mehra, *Expert Opin. Drug Delivery*, 2013, **10**, 353–367.
- 17 C. P. Thakur, A. K. Pandey, G. P. Sinha, S. Roy, K. Behbehani and P. Olliario, *Trans. R. Soc. Trop. Med. Hyg.*, 1996, **90**, 319–322.
- 18 S. Asthana, P. K. Gupta, A. K. Jaiswal, A. Dube and M. K. Chourasia, *Pharm. Res.*, 2015, **32**, 2663–2377.
- 19 E. Dalle Vedove, G. Costabile and O. M. Merkel, *Adv. Healthc. Mater.*, 2018, **7**, 1701398.
- 20 A. Kaur, S. Jain and A. Tiwary, *Acta Pharm.*, 2008, **58**, 61–74.
- 21 G. Shahnaz, B. J. Edagwa, J. McMillan, S. Akhtar, A. Raza, N. A. Qureshi, M. Yasinzai and H. E. Gendelman, *Nanomedicine*, 2017, **12**, 99–115.
- 22 I. Afzal, H. S. Sarwar, M. F. Sohail, S. Varikuti, S. Jahan, S. Akhtar, M. Yasinzai, A. R. Satoskar and G. Shahnaz, *Nanomedicine*, 2019, **14**, 387–406.
- 23 T. Suciati, P. Rachmawati, E. Soraya, A. B. Mahardhika, R. Hartarti and K. Anggadiredja, *J. Appl. Pharm. Sci.*, 2018, **8**, 1–11.
- 24 J. R. McCombs and S. C. Owen, *AAPS J.*, 2015, **17**, 339–351.



25 L. Zhang and I. R. Tizard, *Immunopharmacology*, 1996, **35**, 119–128.

26 L. Ramamoorthy, M. C. Kemp and I. R. Tizard, *Mol. Pharmacol.*, 1996, **50**, 878–884.

27 A. Djeraba and P. Quere, *Int. J. Immunopharmacol.*, 2000, **22**, 365–372.

28 J. B. Kim, K. Park, J. Ryu, J. J. Lee, M. W. Lee, H. S. Cho, H. S. Nam, O. K. Park, J. W. Song, T. S. Kim and D. J. Oh, *Sci. Rep.*, 2016, **6**, 22608.

29 S. Kumar and R. Kumar, *Carbohydr. Polym.*, 2019, **207**, 460–470.

30 D. Miramon-Ortíz, W. Argüelles-Monal, E. Carvajal-Millan, Y. L. López-Franco and F. M. Goycoolea, *Polymers*, 2019, **11**, 330.

31 S. Bhatia, V. Kumar, K. Sharma, K. Nagpal and T. Bera, *Sci. World J.*, 2014, **2014**, 564573.

32 K. S. Nagarsekar, C. Galdhar, R. Gaikwad, A. Samad and P. V. Devarajan, *Drug Delivery Lett.*, 2014, **4**, 208–220.

33 M. A. Tawfik, M. I. Tadros and M. I. Mohamed, *AAPS PharmSciTech*, 2018, **19**, 3650–3660.

34 C. Shu, T. Li, W. Yang, D. Li, S. Ji and L. Ding, *R. Soc. Open Sci.*, 2018, **5**, 171814.

35 G. Schwartzman, I. Asher, V. Folen, W. Brannon and J. Taylor, *J. Pharm. Sci.*, 1978, **67**, 398–400.

36 P. Aggarwal, J. B. Hall, C. B. McLeland, M. A. Dobrovolskaia and S. E. McNeil, *Adv. Drug Delivery Rev.*, 2009, **61**, 428–437.

37 L. Guerrini, R. Alvarez-Puebla and N. Pazos-Perez, *Materials*, 2018, **11**, 1154.

38 K. Hac-Wydro and P. Dynarowicz-Latka, *Biophys. Chem.*, 2006, **123**, 154–161.

39 P. A. Todke and P. V. Devarajan, *J. Controlled Release*, 2022, **349**, 756–764.

40 L. Yang, Y. Sha, Y. Wei, H. Fang, J. Jiang, L. Yin, Z. Zhong and F. Meng, *Biomater. Sci.*, 2023, **11**, 2211–2220.

41 E. Marette, L. Costantino, F. Buttini, C. Rustichelli, E. Leo, E. Truzzi and V. Iannuccelli, *Drug Delivery Transl. Res.*, 2019, **9**, 298–310.

42 I. D. Zlotnikov, M. A. Vigovskiy, M. P. Davydova, M. R. Danilov, U. D. Dyachkova, O. A. Grigorieva and E. V. Kudryashova, *Int. J. Mol. Sci.*, 2022, **23**, 16144.

43 V. Liévin-Le Moal and P. M. Loiseau, *FEBS Lett.*, 2016, **283**, 598–607.

44 J. G. Visser, A. D. P. Van Staden and C. Smith, *Front. Pharmacol.*, 2019, **10**, 22.

45 P. Sawangchan, F. A. Júnior, É. N. Alencar, E. S. Egito and L. E. Kirsch, *Int. J. Pharm.*, 2023, **632**, 122586.

46 K. C. Nicolaou, T. K. Chakraborty, Y. Ogawa, R. A. Daines, N. S. Simpkins and G. T. Furst, *J. Am. Chem. Soc.*, 1988, **110**, 4660–4672.

47 S. Axelrod, H. Oschkinat, J. Enders, B. Schlegel, V. Brinkmann, S. H. Kaufmann, A. Haas and U. E. Schaible, *Cell. Microbiol.*, 2008, **10**, 1530–1545.

48 A. M. Pauwels, M. Trost, R. Beyaert and E. Hoffmann, *Trends Immunol.*, 2017, **38**, 407–422.

49 Y. Kao and R. Juliano, *Biochim. Biophys. Acta*, 1981, **677**, 453–461.

50 R. L. Souhami, H. M. Patel and B. E. Ryman, *Biochim. Biophys. Acta*, 1981, **674**, 354–371.

51 J. Dave and H. M. Patel, *BBA, Biochim. Biophys. Acta, Mol. Cell Res.*, 1986, **888**, 184–190.

52 L. Li, W. Xu, Y. Luo, C. Lao, X. Tong, J. Du, B. Huang, D. Li, J. Chen, H. Ye and F. Cong, *Carbohydr. Polym.*, 2022, **297**, 120032.

53 T. J. McDonnell, S. W. Chang, J. Y. Westcott and N. F. Voelkel, *J. Appl. Physiol.*, 1988, **65**, 2195–2206.

